C. Kwok

Waves in discrete spatial domains

Bachelor's thesis, August 25, 2013

Supervisor: Dr. H.J. Hupkes

Mathematisch Instituut, Universiteit Leiden

Contents

1 Introduction

Modelling spatial discreteness occurs in many areas of science and engineering. This thesis focuses on the propagation of signals through nerve fibers. Such fibers are coated with myelin sheaths and admits gaps at the so-called nodes of Ranvier. There, ions can exit and enter the fiber. In 1952, Hodgkin and Huxley described how action potentials propagates through a squid giant axon. However, the Hodgkin-Huxley equations are rather complicated. FitzHugh proposed a simpler model and this model was further studied by Nagumo and has become known as the FitzHugh-Nagumo equation. Theoretically, not everything is understood and there is not much work done numerically. This thesis explores the issues encountered when doing such numerical research.

First, we discuss the discrete Nagumo equation in section 3:

$$\frac{dV_i}{dt} = \alpha[V_{i+1} + V_{i-1} - 2V_i] - (V_i + 1)(V_i - 1)(V_i - \rho),$$

with V_i representing the potential in node i, $\alpha = h^2$ with h the distance between two consecutive nodes and ρ a constant between -1 and 1. By looking at the waves that connect the points -1 and 1, we find a relation between α, ρ and the wavespeed c numerically. The numerical methods used in the simulations are the collocation method and Newton's method which are described in section 3.1.

Secondly, the FitzHugh-Nagumo equations given by

$$\begin{aligned} \dot{V}_j(t) &= \alpha[V_{j+1} + V_{j-1} - 2V_j] + V_j(1 - V_j)(V_j - a) - W_j \\ \dot{W}_j(t) &= \varepsilon(V_j - \gamma W_j), \end{aligned}$$

with W_j representing the recovery component, γ a constant, $\varepsilon << 1$ a constant and a a constant between 0 and 1, will be examined and the profile of the waves are to be explained in section 4. The difficulties encoutered when simulating are discussed in section 4.1 and the results of the simulations are given in section 4.2. We will see a relation between ε, a and c. It is only known rigorously that there exists waves, ie solutions, under certain conditions. However, we find in the numerical results that there are also solutions which do not meet the conditions.

Elmer and van Vleck have also done some research with the FitzHugh-Nagumo equations, see [14]. However, they used a different nonlinear function and it turns out that there is a difference in our results. This will be discussed in 4.3.

2 Biological background

There are nerve fibers in our body which are about a meter long. A signal through a fiber must cover this distance. Luckily this happens in an instant. For example it enables you to pull your hand away quickly when your hand touches something extremely hot by accident. The reason why such a signal can travel so fast is because the signal in the fiber actually jumps through it.

A fiber is shown in figure 1. It consists of alternately myelin sheaths and nodes of Ranvier. Myelin sheaths are made of an isolating substance which prevents the passage of ions. In contrast to myelin sheats are the nodes of Ranvier where ions can acces and leave the fiber. The distance between two consecutive nodes depends on the diameter of the fiber and lies between $0.3mm$ and $2mm$, [1].

The concentration of sodium ions outside the fiber is a lot higher than inside the fiber. As for the concentration of potassium ions it is the other way around. This difference in concentration is maintained by energy consuming ion pumps at the nodes of Ranvier. However, the transport of sodium ions is quicker than that of the potassium ions, resulting in a negative potential of the fiber in rest of approximately $-70mV$.

Due to the influence of a neurotransmitter or an approaching impulse the potential can rise. When this exceeds the threshold of approximately $-55mV$, the permeability of sodium ions increases. Consequently, voltage-gated ion channels become activated which leads to a further rise of the potential until it reaches about $+40mV$. Then, the permeability of sodium ions decreases and the permeability of potassium ions increases. The latter leaves the fiber which leads to a decrease of the potential. Since the potassium channels do not respond that quickly, the potential becomes slightly more negative than its resting potential. Subsequently, the permeability of the membrane returns to normal and the potassium ions and sodium ions are pumped back to their positions, [2]. This proces is called an action potential and is shown in figure 2.

The sodium ions which have entered the fiber move to the next node of Ranvier since the potential is more negative there. This results in an action potential at the next node. Thus, we have a signal which penetrates the fiber. Since the exchange of ions only takes place at the nodes, the action potential jumps from node to node, resulting in a wave propagating through a discrete spatial domain. This is the reason why a signal can travel a great distance in a very short period of time. When the fibers do not contain myelin sheats, the signal does not jump and will travel at a much slower speed. The difference between the speeds can lead up to $120m/s$, [3].

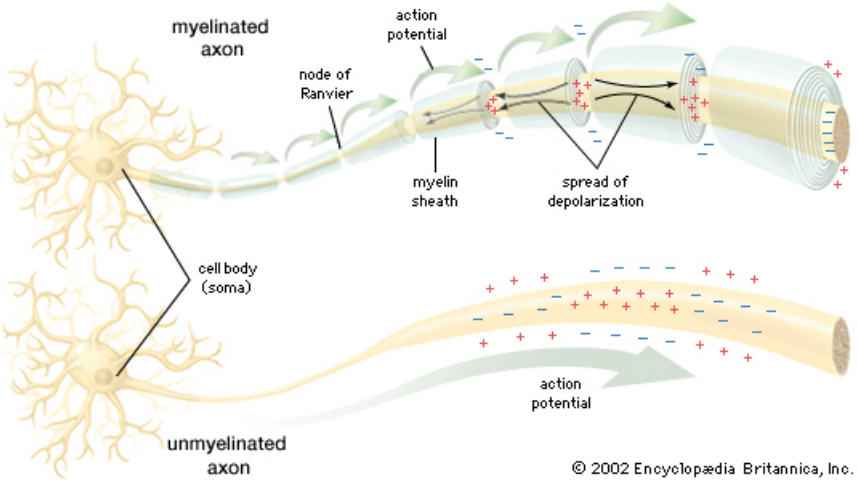

Fig. 1: A myelinated nerve fiber with nodes of Ranvier.[1]

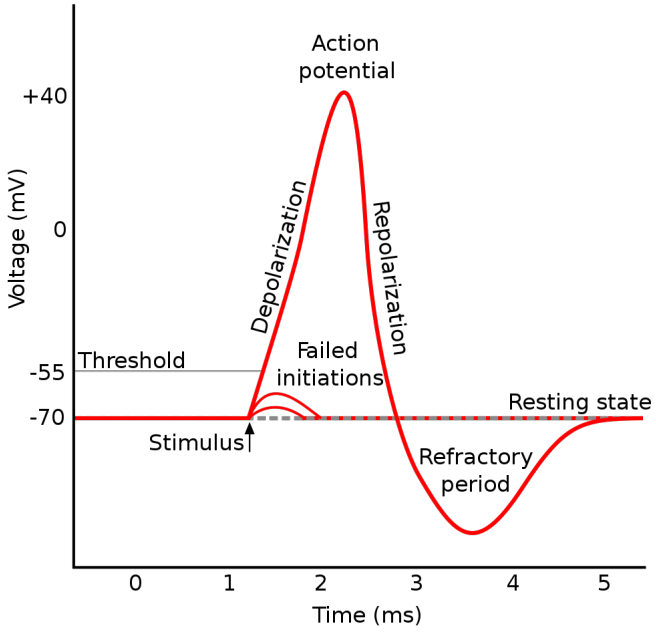

Fig. 2: Schematic of an action potential.[2]

[1] Copyright Britannica. Displayed under their Terms of Use. http://www.britannica.com/EBchecked/topic/417103/node-of-Ranvier

[2] Original author: Chris 73. Updated by Diberri. Copied under the terms of the GNU Free Documentation License. http://commons.wikimedia.org/wiki/File:Action_potential.svg

3 Nagumo equation

A signal jumping through a fiber can thus be seen as a wave travelling through a discrete spatial domain. By using the model given by the Nagumo equation (3.1), we want to observe what kind of effect changing the distance between two consecutive nodes have on the shape and speed of such a wave. This model is as follows

$$\frac{dV_i}{dt} = h^{-2}[V_{i+1} + V_{i-1} - 2V_i] - g(V_i, \rho), \tag{3.1}$$

with V_i a function of time t and representing the potential in node i, h the distance between two consecutive nodes and $g(V_i, \rho) = (V_i + 1)(V_i - 1)(V_i - \rho)$ with ρ a constant between -1 and 1. We look at the states in which all the nodes have the same potential, thus for all i holds $V_i = V$ for some potential $V \in \mathbb{R}$. Then the following holds:

$$\frac{dV_i}{dt} = -g(V_i, \rho) \tag{3.2}$$

The roots of $g(V_i, \rho)$ are $1, -1$ and ρ, thus the whole system is in rest if V is equal to $1, -1$ or ρ. Since the dynamics are stable for the points $V = \pm 1$ and unstable for $V = \rho$, we have a bistable system. There exists a competition between the discretization of the diffusion term and the nonlinearity. The result of this competition is a formation of a travelling wave, [4].

Such traveling waves have a constant shape ϕ, speed c, and connect the points -1 and 1. We apply the travelling wave ansatz $V_i(t) = \phi(i - ct)$. This results in the following equation

$$-c\phi'(\xi) = \alpha[\phi(\xi+1) + \phi(\xi-1) - 2\phi(\xi)] - (\phi(\xi)+1)(\phi(\xi)-1)(\phi(\xi)-\rho), \tag{3.3}$$

with $\alpha = h^{-2}$ and $\xi = i - ct$. The boundary conditions imposed are

$$\lim_{\xi \to -\infty} \phi(\xi) = -1, \qquad \lim_{\xi \to \infty} \phi(\xi) = 1. \tag{3.4}$$

The differential equation (3.3) is called a differential equation of mixed type since $\phi'(\xi)$ is dependent on the value of ϕ at $\xi - 1$ and $\xi + 1$. The following theorem states that there are solutions to (3.3) with an unique wavespeed and such solutions are unique when $c \neq 0$.

Theorem 3.1. *Let*

$$-c\phi'(\xi) = \alpha[\phi(\xi+1) + \phi(\xi-1) - 2\phi(\xi)] - f(\phi, \rho) \tag{3.5}$$

$$\lim_{\xi \to -\infty} \phi(\xi) = r_1, \qquad \lim_{\xi \to \infty} \phi(\xi) = r_2 \tag{3.6}$$

with $\alpha > 0$ and $f(\phi, \rho)$ a polynomial of degree three. Let its roots be r_1, ρ, r_2 with $r_1 < \rho < r_2$ and $f(\phi, \rho) < 0$ if $\phi \in (-\infty, r_1) \cup (\rho, r_2)$ and $f(\phi, \rho) > 0$ if $\phi \in (r_1, \rho) \cup (r_2, \infty)$. Then for every $\rho \in (r_1, r_2)$, there exists $c \in \mathbb{R}$, and a monotone increasing solution $\phi = P(\xi)$ of (3.5) on $\mathbb{R}$ satisfying the boundary conditions (3.6). This $c = c(\rho) \in \mathbb{R}$ is unique, and depends continuously on ρ, and is C^1 smoothly on ρ when $c(\rho) \neq 0$. If $c(\rho) \neq 0$ then the solution P is unique up to translation among all solutions satisfying (3.4) and also satisfies $P'(\xi) > 0$ with $\xi \in \mathbb{R}$.

Proof. See [5]. □

One of the effects of ρ in (3.3) is determining in which direction the wave will travel. Observe the case where the distance between the nodes goes to zero, thus the limit $h \to 0$. This results in the following PDE

$$u_t = u_{xx} - (u+1)(u-1)(u-\rho). \tag{3.7}$$

If we look at the travelling wave solutions of (3.7), we find the following second-order differential equation

$$-c\phi' = \phi'' - (\phi+1)(\phi-1)(\phi-\rho). \tag{3.8}$$

This can be solved explicitly. We find:

$$\phi(\xi) = \tanh(\frac{1}{2}\sqrt{2}\xi) \tag{3.9}$$

$$c = \sqrt{2}\rho \tag{3.10}$$

If $\rho \in (-1,0)$, then the wave travels to the left. If $\rho \in (0,1)$, then the wave travels to the right. Only when ρ is equal to 0, the wave will stand still, in other words $c = 0$ and we speak of propagation failure. In our case, ρ still determines in which direction the wave will travel. However, it can now occur that the wave is standing still even though ρ is not zero.

3.1 Numerical methods

The model in (3.3) can be simulated by using a special written program in Fortran 95 which can simulate differential equations of mixed type, see [6] for more information. Programs such as AUTO, [7], are not suited to simulate this, since we do not have ordinary differential equations. Using DDE-biftool, [8], will also not work, since it can only simulate equations with delay terms and not advanced terms and we have both.

The numerical methods used are the collocation method and Newton's method. By using the collocation method, we get a system with unknown variables. This can be solved numerically by using Newton's method. However, using this method, a starting solution is required.

Example 1. Let

$$y'(x) = y(x), \tag{3.11}$$

with the boundary condition $y(0) = 1$ and $x \in [0,1]$. Assume y is a polynomial of second degree, thus $y = ax^2 + bx + c$ with a, b, and c constants. Then take two points in $[0,1]$, so called collocation points, for example $\frac{1}{3}$ and $\frac{2}{3}$ for which (3.11) must hold. Then, the following must hold:

$$y(0) = 1 \tag{3.12}$$

$$y(\frac{1}{3}) = y'(\frac{1}{3}) \tag{3.13}$$

$$y(\frac{2}{3}) = y'(\frac{2}{3}) \tag{3.14}$$

Thus, we find the following system of equations:

$$c = 1 \tag{3.15}$$

$$\frac{1}{9}a + \frac{1}{3}b + c = \frac{2}{3}a + b \tag{3.16}$$

$$\frac{4}{9}a + \frac{2}{3}b + c = \frac{4}{3}a + b \tag{3.17}$$

When solving (3.11) analytically, we find $y = e^x$. Note, the series expansion at $x = 0$ is $1 + x + \frac{1}{2}x^2$. From (3.15),(3.16) and (3.17), we find $a = \frac{9}{11}$, $b = \frac{9}{11}$ and $c = 1$. Thus, an approximation of y is $y \approx \frac{9}{11}x^2 + \frac{9}{11}x + 1$.

In our case, we must solve the following

$$-c\phi'(\xi) = \alpha\left[\phi(\xi+1) + \phi(\xi-1) - 2\phi(\xi)\right] - (\phi(\xi)+1)(\phi(\xi)-1)(\phi(\xi)-\rho) \tag{3.18}$$

$$c'(\xi) = 0 \tag{3.19}$$

with $\xi \in [L_l, L_r]$ and $L_l, L_r \in \mathbb{R}$. Since c is unknown, solving (3.19) simultaneously with (3.18) gives both the solution ϕ and c. By following the approach of [9], we introduce an artificial diffusion term $\gamma\phi''$, giving

$$\begin{aligned} 0 &= \gamma\phi''(\xi) + c\phi'(\xi) + \alpha\left[\phi(\xi+1) + \phi(\xi-1) - 2\phi(\xi)\right] \\ &\quad -(\phi(\xi)+1)(\phi(\xi)-1)(\phi(\xi)-\rho), \end{aligned} \tag{3.20}$$

$$c'(\xi) = 0. \tag{3.21}$$

The value of γ is of the order $\gamma = 10^{-5}$. Since $\xi \in [L_l, L_r]$, the boundary conditions are

$$\phi(L_l) = -1, \tag{3.22}$$

$$\phi(L_r) = 1, \tag{3.23}$$

$$\phi(0) = 0. \tag{3.24}$$

The last boundary condition is to have the solutions normalized. The equation (3.20) can be written as

$$\begin{aligned} \phi''(\xi) &= -\frac{1}{\gamma}(c\phi(\xi) + \alpha\left[\phi(\xi+1) + \phi(\xi-1) - 2\phi(\xi)\right] \\ &\quad -(\phi(\xi)+1)(\phi(\xi)-1)(\phi(\xi)-\rho)) \end{aligned} \tag{3.25}$$

The right-hand side of (3.25) is a nonlinear function, making the system of equations such as in (3.15), (3.16) and (3.17) more complicated. Thus, Newton's method is used to solve this. Note, since ϕ' is dependent on the shifts $\phi(\xi+1)$ and $\phi(\xi-1)$, determining the inverse of the matrix in Newton's method is very difficult. Thus, this is all done numerically.

3.2 Numerical results

By simulating (3.25), (3.21) with (3.22), (3.23) and (3.24) we find the following graphs.

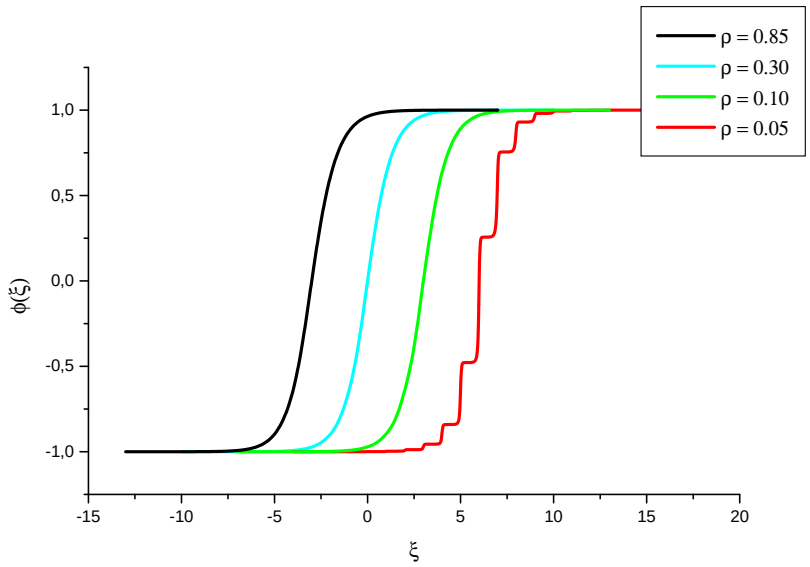

Fig. 3: Wave profiles $\phi(\xi)$ at different values of ρ with $\alpha = 1$. The curves have been shifted for presentation purposes.

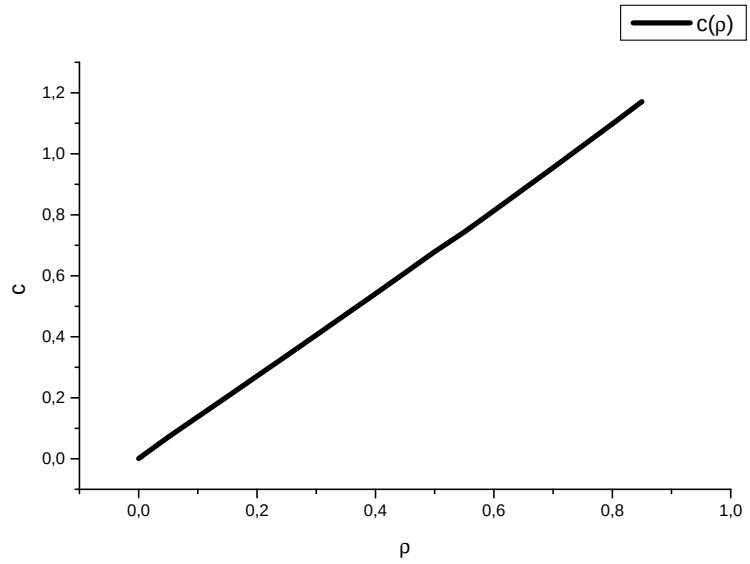

Fig. 4: Wavespeed c against ρ with $\alpha = 1$.

In figure 3, we see that when the parameter ρ decreases to 0.05, the waveprofile starts to lose its smoothness.

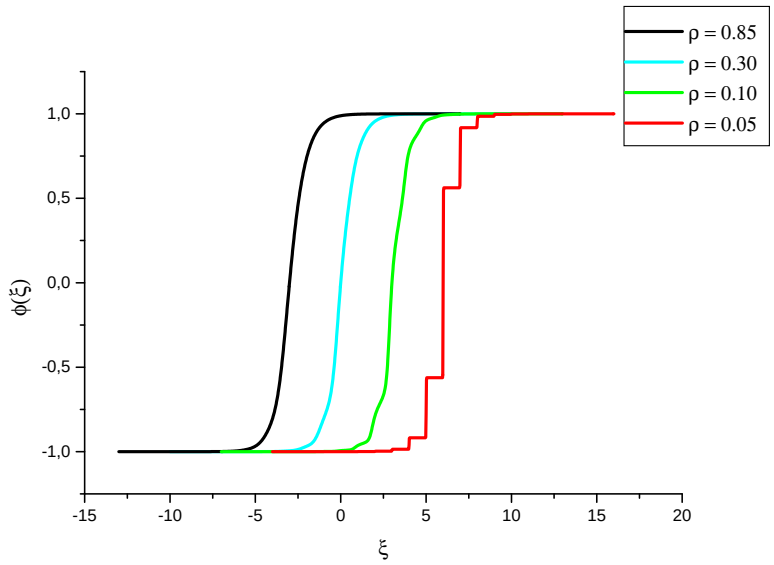

Fig. 5: Wave profiles $\phi(\xi)$ at different values of ρ with $\alpha = 0.5$. The curves have been shifted for presentation purposes.

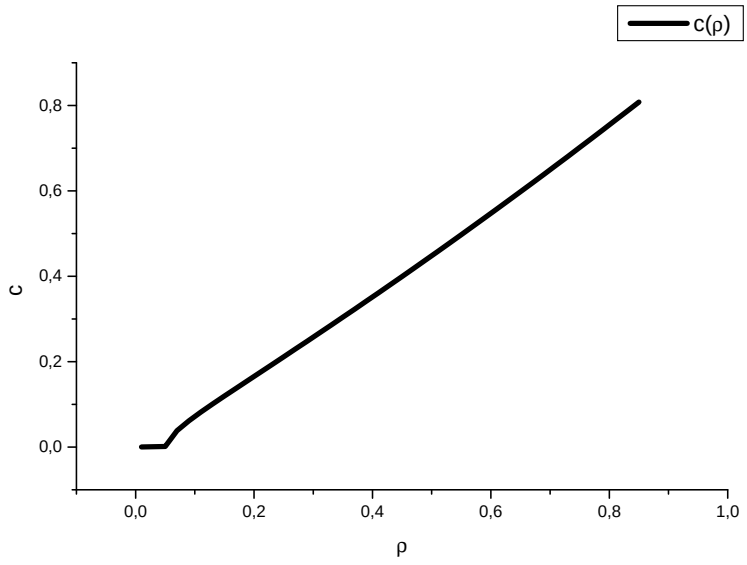

Fig. 6: Wavespeed c against ρ with $\alpha = 0.5$.

In figure 5, the value of α is 0.5, which is smaller than in figure 3. Notice that as the parameter ρ is decreased, the waveprofiles begins to lose their smoothness at $\rho = 0.1$ and is a step function at $\rho = 0.05$ as opposed to figure 3.

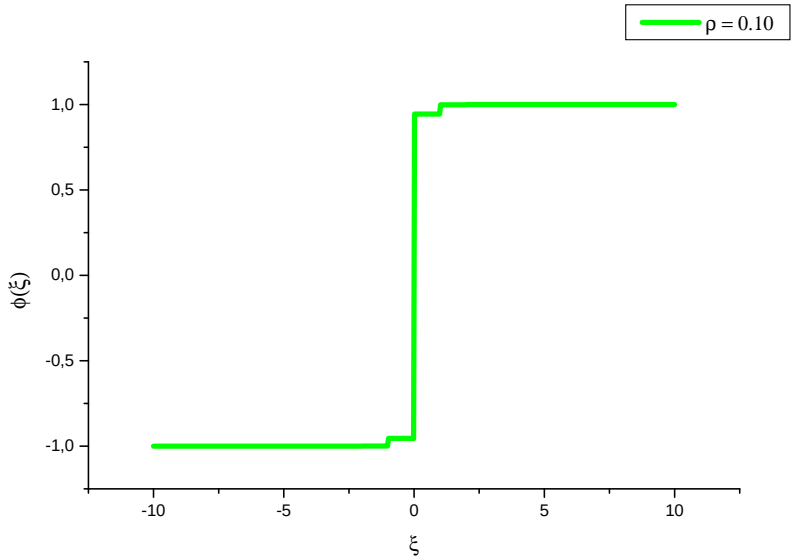

Fig. 7: Wave profile $\phi(\xi)$ at $\rho = 0.1$ with $\alpha = 0.05$.

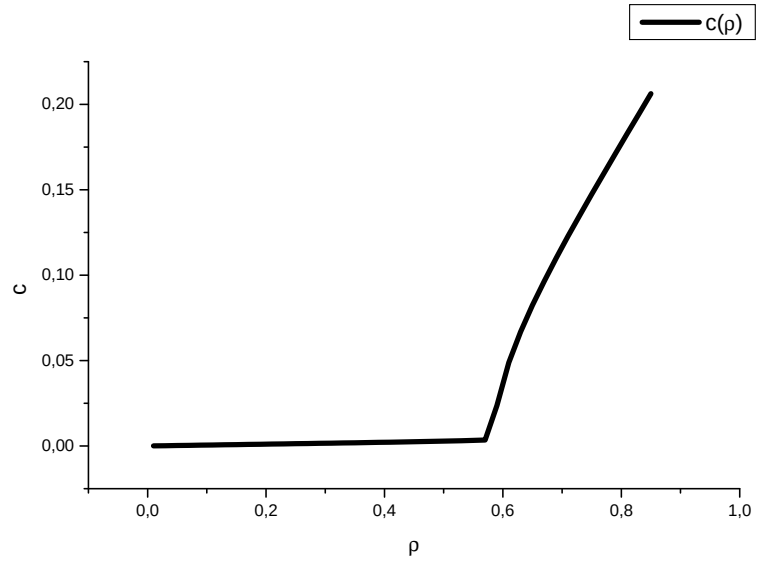

Fig. 8: Wavespeed c against ρ with $\alpha = 0.05$.

In figure 7, the value of α is 0.05. The waveprofile of $\rho = 0.1$ has lost all its smoothness and has become a step function.

Observe figure 4, 6 and 8. The interval for which $c = 0$ holds, becomes larger as α decreases. Also, there are values of ρ unequal to zero for which $c = 0$ holds in contrast to the continuous case. Define ρ^* as the largest ρ such that $c = 0$ holds. In figure 8 this would be the sharp point in the graph. In figure 9, it is shown that ρ^* increases as α decreases. According to theorem 2.6 in [5], $\rho^* < 1$ holds. However, Keener has shown in chapter 2 in [11] that $\lim_{\alpha \to 0} \rho^* = 1$ holds.

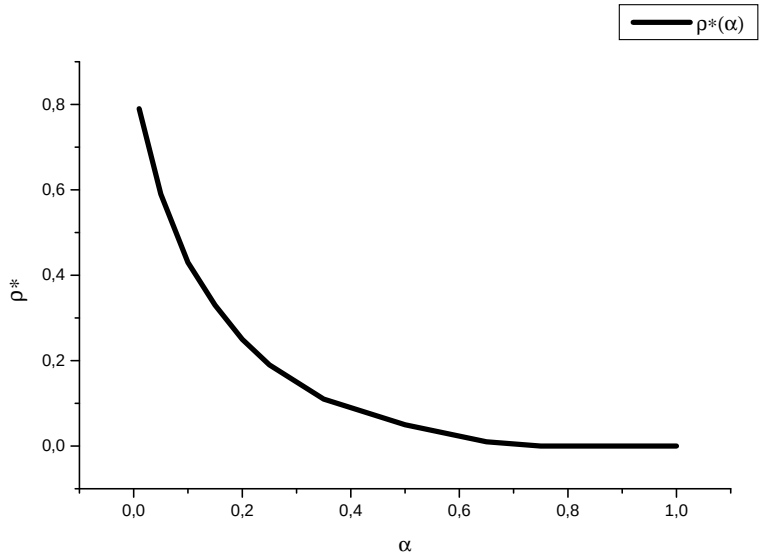

Fig. 9: ρ^* against α.

4 FitzHugh - Nagumo equations

Another model describing the excitations of a nerve is given by the FitzHugh - Nagumo equations. This model is a bit more complicated then (3.1), but it is more realistic. In this case, there is a pulse. The system returns to an equilibrium after being disturbed and the behaviour is described as a relaxation oscillator. The model is as follows

$$\dot{V}_j(t) = \alpha[V_{j+1} + V_{j-1} - 2V_j] + g(V_j, a) - W_j \tag{4.1}$$
$$\dot{W}_j(t) = \varepsilon(V_j - \gamma W_j), \tag{4.2}$$

with V_j still the potential in node j, $\alpha = h^{-2}$, with h the distance between two consecutive nodes and $g(V_j, a) = V_j(1 - V_j)(V_j - a)$, with $a \in (0, 1)$. The variable W_j represents the recovery component of node j (a slow variable). γ is a positive constant and $0 < \varepsilon << 1$ accounts for the slow kinetics of the sodium channel.

The $\mathcal{O}(1)$, ie fast time scale, equations in (4.1) and (4.2) are

$$\dot{V}_j(t) = \alpha[V_{j+1} + V_{j-1} - 2V_j] + g(V_j, a) - W_j, \tag{4.3}$$
$$\dot{W}_j(t) = 0. \tag{4.4}$$

The $\mathcal{O}(\varepsilon)$, ie slow time scale, equation in (4.2) is

$$\dot{W}_j(t) = \varepsilon(V_j - \gamma W_j). \tag{4.5}$$

We can now analyze the profiles of both the waves. Observe figure 11. By looking for spatially constant equilibria for the fast time scale, thus $V_j = V_{j+1} = V_{j-1}$ holds, we find $\dot{V}_j(t) = 0$ when $W_j = g(V_j, a)$. Thus, the equilibrium points of the fast time scale are given by the red graph $W_j = g(V_j, a)$.

The arrows on this graph describe the behaviour in time for $\mathcal{O}(\varepsilon)$. We see that $\dot{W}_j(t) < 0$ holds for the left side of the line $V_j = \gamma W_j$ and $\dot{W}_j(t) > 0$ for the right side of the line using (4.5), thus the arrows correspond to how W_j changes in time. We assume that V_j always goes to an equilibrium value instantly on the slow time scale. However, since W_j changes on the slow time scale and we can see V_j as a function of W_j, V_j also changes on the slow time scale. For W_j on the purple part of the graph in figure 10, we have $V_j = h_l(W_j)$ with $h_l(W_j)$ the inverse of $W_j = g(V_j, a)$ on that part. Thus,

$$\dot{W}_j = \varepsilon(h_l(W_j) - \gamma W_j) \tag{4.6}$$

holds for W_j in the slow time scale on the purple part. For W_j on the light blue part, we have $V_j = h_r(W_j)$ with $h_r(W_j)$ the inverse of $W_j = g(V_j, a)$ on that part. Thus,

$$\dot{W}_j = \varepsilon(h_r(W_j) - \gamma W_j) \tag{4.7}$$

holds for W_j in the slow time scale on the light blue part.

Since (4.4) holds, we can take W_j as a constant for the fast time scale. Then (4.3) can be written in the form such as (3.1), but with a different polynomial of degree three. By following the same approach as in section 3, we can apply

theorem 3.1. Thus, there exists a wave called the front that connects $V_j = 0$ and $V_j = 1$. This is the green graph in figure 11. The cubic is symmetric around the point $(v_{\text{mir}}, w_{\text{mir}})$. We mirror W_j to $W_j^{(m)}$ and V_j to $V_j^{(m)}$ with

$$V_j^{(m)} = v_{\text{mir}} - (V_j - v_{\text{mir}}), \tag{4.8}$$

$$W_j^{(m)} = w_{\text{mir}} - (W_j - w_{\text{mir}}). \tag{4.9}$$

This mirrors the front in a wave called the back, which is the yellow graph. The double arrows describe the behaviour on the fast time scale.

The solution is periodic and the trajectory through one cycle is given by the blue graph. How smaller ε is, how closer the graph follows the path given by (I),(II),(III) and (IV). This path consists of two fast components and two slow components. Together they form what is known as a relaxation oscillation.

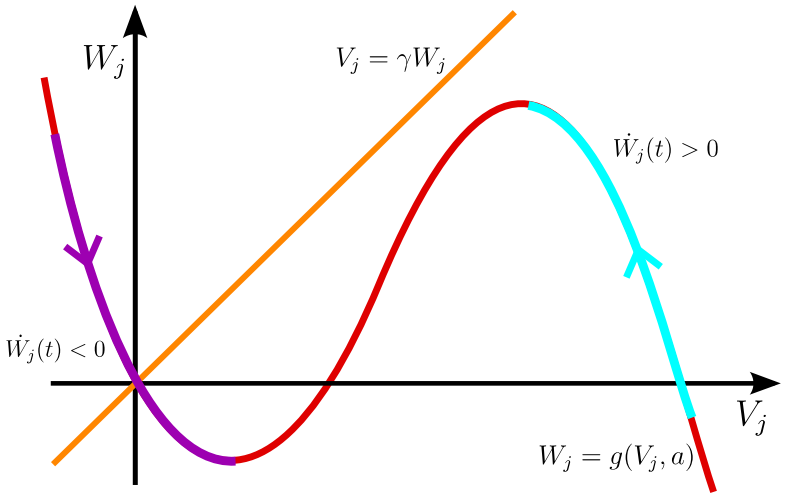

Fig. 10: The graph $W_j = g(V_j, a)$.

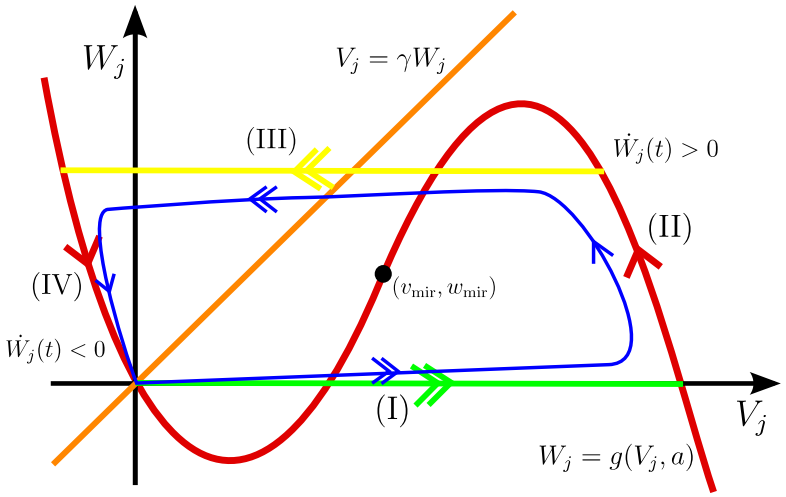

Fig. 11: Phase portrait of FitzHugh-Nagumo model.

By applying the travelling wave ansatz $(V_j, W_j)(t) = (v, w)(j - ct)$ and letting $\xi = j - ct$, we get the following equations

$$\begin{aligned} -cv'(\xi) &= \alpha[v(\xi+1) + v(\xi-1) - 2v(\xi)] \\ &\quad + v(\xi)(1 - v(\xi))(v(\xi) - a) - w(\xi) \qquad (4.10) \\ -cw'(\xi) &= \varepsilon(v(\xi) - \gamma w(\xi)) \qquad (4.11) \end{aligned}$$

with

$$\lim_{\xi \to -\infty} v(\xi) = 0, \qquad \lim_{\xi \to \infty} v(\xi) = 0 \qquad (4.12)$$

$$\lim_{\xi \to -\infty} w(\xi) = 0, \qquad \lim_{\xi \to \infty} w(\xi) = 0 \qquad (4.13)$$

as the boundary conditions. Notice that (4.10) and (4.11) are both differential equations of mixed type. The following theorem states that there are solutions to (4.10) and (4.11).

Theorem 4.1. *Consider* (4.10) *and* (4.11)*, then for each* $c > c_*$ *with* $c_* < 0$ *the wavespeed belonging to the Nagumo wave equation*

$$-c_* v'(\xi) = \alpha[v(\xi+1) + v(\xi-1) - 2v(\xi)] + v(\xi)(1 - v(\xi))(v(\xi) - a) \qquad (4.14)$$

with $\alpha > 0$ *and* c *sufficiently close to* c_**, there exists a unique* $\varepsilon = \varepsilon(c) > 0$ *for which* (4.10) *and* (4.11) *admit a solution* (v, w)*. This pair* (v, w) *is* $\mathcal{O}(c + c_*)$*-close to the singular orbit that arises by combining the orbits (I)-(IV) in figure 11 and is unique up to translations.*

Proof. See [10]. Note the ansatz used in [10] is $(V_j, W_j)(t) = (v, w)(j + ct)$, thus the c used in this thesis is equal to their $-c$. □

So we have solutions (v, w) to (4.10) and (4.11) if the wavespeed c is close to the wavespeed c_* belonging to the Nagumo wave equation. However, we will see in section 4.2 that there are also solutions in which c is not close to c_*.

4.1 Numerical difficulties

When trying to simulate the model given by (4.10) and (4.11) multiple problems occured. Using the same starting solution as the one used in the Nagumo model does not work. This is because the starting solution differs too much from the real solution. Thus, a more accurate starting solution is needed. By using the model in [12], which is continuous and has a different nonlinearity, solutions belonging to that model were found. Then discrete terms were added to the equation. By putting a factor S in front of the continuous part and a factor $1 - S$ in front of the discrete part, it was possible to give the discrete part more weight then the continuous part in each iteration. This was done by setting $S = 1$ at the beginning and increasing S in each iteration until S was (almost) 0. The same was done with the different nonlinearity. Consequently, we obtained a more accurate starting solution for the following system

$$\begin{aligned} -cv'(\xi) &= \alpha[v(\xi+1) + v(\xi-1) - 2v(\xi)] \\ &\quad +B(v(\xi)(1-v(\xi))(v(\xi)-a)) - w(\xi) \qquad (4.15) \\ -cw'(\xi) &= \varepsilon(v(\xi) - \gamma w(\xi)), \qquad (4.16) \end{aligned}$$

with $B \approx 3.3814$. Notice we have a factor B in front of the nonlinearity, but this does not have a big effect on our research.

Another problem is that the interval in which the solutions are located was dependent on the value of ε. If ε is small, then the interval in which the solutions are given would become larger. The reason for this to happen is that ε determines how fast the slow time scale is and the period of the solution is determined by the slow time scale. Thus, if ε is small, the period of the solutions would become larger resulting in a larger interval. This is not very practical. This can be solved by scaling the solutions, making the solutions fit in the interval $[0, 1]$. Therefore we introduce $s(\varepsilon)$ with the new scaled solutions $\tilde{v}(\frac{\xi}{s}) = v(\xi)$ and $\tilde{w}(\frac{\xi}{s}) = w(\xi)$. The speed c is not affected by the scaling and thus remains the same.

Just as in section 3.1 we introduce artificial diffusion term $\delta\tilde{v}$ and $\delta\tilde{w}$, giving the system we want to solve

$$\begin{aligned} \tilde{v}(\tilde{\xi})'' &= -\frac{s^2}{\delta}(c\frac{\tilde{v}'(\tilde{\xi})}{s} + \alpha[\tilde{v}(\tilde{\xi}+1) + \tilde{v}(\tilde{\xi}-1) - 2\tilde{v}(\tilde{\xi})] \\ &\quad +B(\tilde{v}(\tilde{\xi})(1-\tilde{v}(\tilde{\xi}))(\tilde{v}(\tilde{\xi})-a)) - \tilde{w}(\tilde{\xi})), \qquad (4.17) \\ \tilde{w}(\tilde{\xi})'' &= -\frac{s^2}{\delta}(c\frac{\tilde{w}'(\tilde{\xi})}{s} + \varepsilon(\tilde{v}(\tilde{\xi}) - \gamma\tilde{w}(\tilde{\xi}))), \qquad (4.18) \\ c'(\tilde{\xi}) &= 0, \qquad (4.19) \end{aligned}$$

with $\tilde{\xi} = \frac{\xi}{s}$ and $\delta = 10^{-5}$. The boundary conditions are

$$v(0) = 0, \qquad v(1) = 0, \tag{4.20}$$

$$w(0) = 0, \qquad w(1) = 0, \tag{4.21}$$

$$v(\frac{1}{3}) = \frac{1}{4}. \tag{4.22}$$

The last boundary condition eliminates the trivial solution $v \equiv 0 \equiv w$.

In [13], where the model was continuous, each a corresponds to two wavespeeds. Thus, this is also suspected in the discrete case. Thereby, it was not sufficient to only vary a in each iteration when observing the effect of a on c. This can be solved, by varying c in each iteration.

4.2 Numerical results

The following results were found numerically. The values of α and γ are 1 and 0.8 respectively in all the simulations. The scaling that was used is $s = \frac{8}{\varepsilon}$. In figure 12, the profiles of both the waves are shown. The solutions travel to the right. Thus, the potential for V_j grows quickly first, followed by a slow decrease and then a fast decrease in which the potential even becomes negative and finaly increasing slowly until it reaches zero again. The potential of W_j barely changes when the potential V_j changes quickly, but it slowly grows when that of V_j decreases and slowly decreases when that of V_j increases. This corresponds to the analytically theory discussed at the beginning of chapter 4.

Increasing B in (4.15) to $1.75 \times B \approx 10.32$ and simulating

$$\begin{aligned} -cv'(\xi) &= \alpha[v(\xi+1) + v(\xi-1) - 2v(\xi)] \\ &\quad +B(v(\xi)(1-v(\xi))(v(\xi)-a)), \end{aligned} \tag{4.23}$$

which is the Nagumo equation with solutions that are waves connecting 0 and 1, we see in figure 13 that there is propagation failure for some a. Notice that the graph in 13 is reflected over the a-axis. This is done for presentation purposes.

In figure 14, the relationship between a and c are plotted for $\varepsilon = 0.02$ and $\varepsilon = 0.08$. Since the boundary conditions of (4.10) and (4.11) are (4.12) and (4.13), if $((v, w)(\xi), c)$ is a solution then $((v, w)(-\xi), -c)$ is also a solution. Thus, the reflection of the Nagumo graph over the a-axis is justified. Notice how close the black en blue graph follow the pink graph, but then make a turn which ensures a second solution of c corresponding to a value of a. After the turn, both the graphs grow in the c-direction slowly. Thus, we have solutions eventhough c is not close to c_*.

The reason why the blue graph stops at the top is because the solutions of v corresponding to the values of c becomes wider as c increases. This can be seen in figure 15. By increasing the scale factor s, this can be solved. It is not known why the black graph stops at the right side. The reason why the blue graph as well as the black graph stops at the left side is that the solution of v shrinks. In figure 16, this can be seen for $\varepsilon = 0.08$. The consequence is that it cannot satisfy the boundary condition (4.22) anymore.

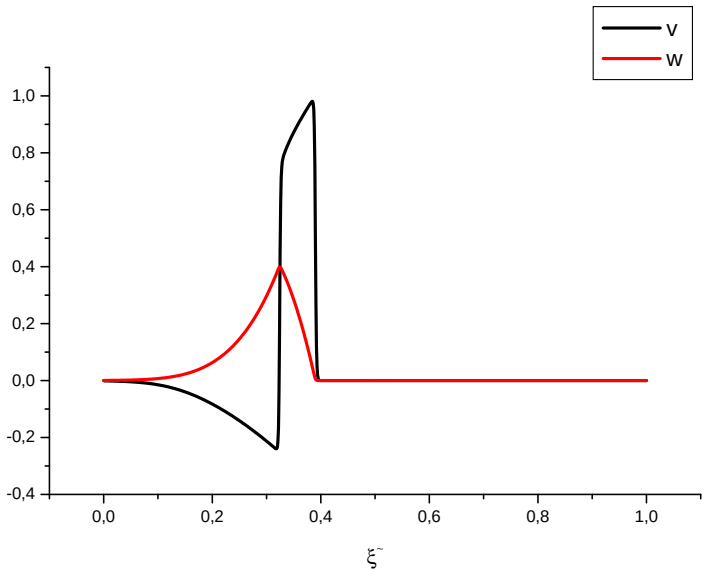

Fig. 12: Wave profiles v and w with $a = 0.01$ and $\varepsilon = 0.01$.

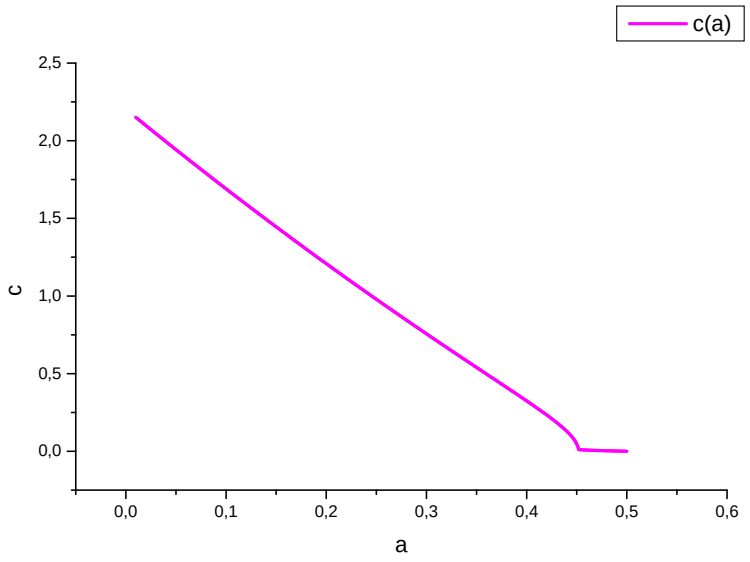

Fig. 13: Wavespeed c (reflected over the a-axis) against a using (4.23).

Observe figure 17, this is the graph with $\varepsilon = 0.02$ in figure 14 zoomed in after the turn. The graph drops a bit before it increases steadily.

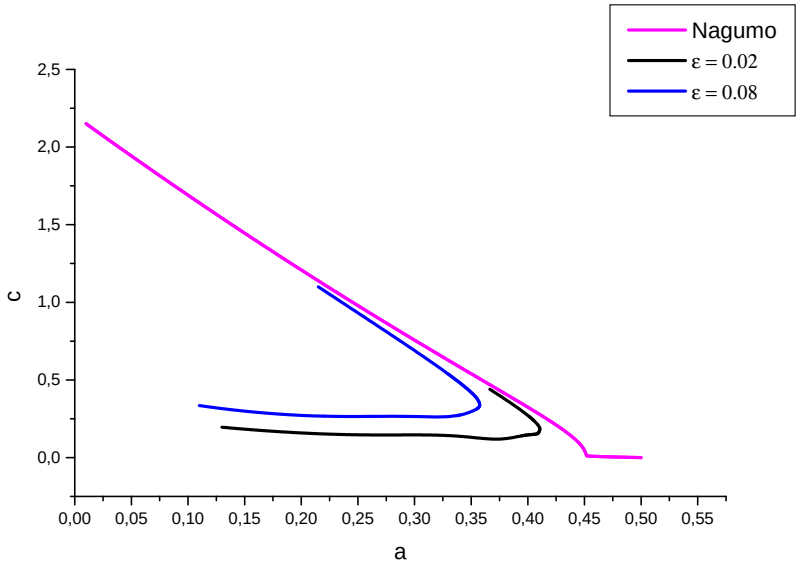

Fig. 14: Wavespeed c against a.[3]

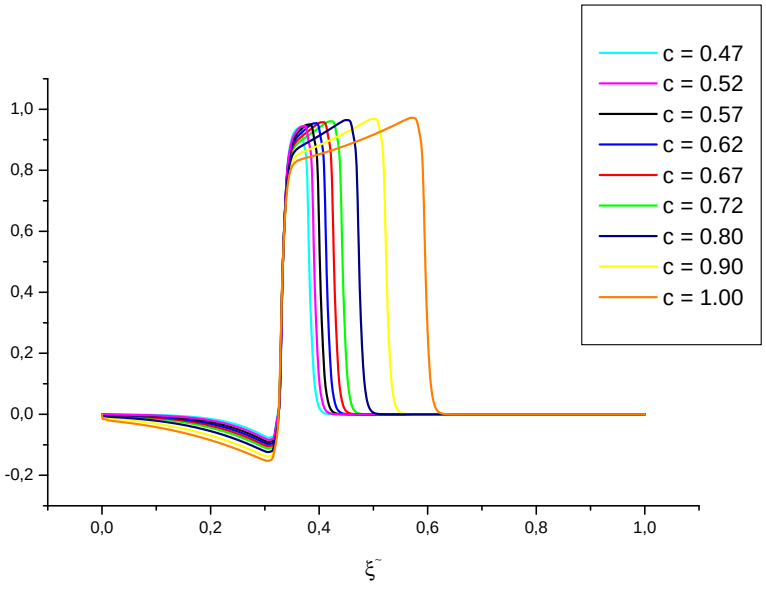

Fig. 15: The waveprofile v for multiple values of c with $\varepsilon = 0.08$.

[3] The Nagumo graph is reflected over the a-axis for presentation purposes.

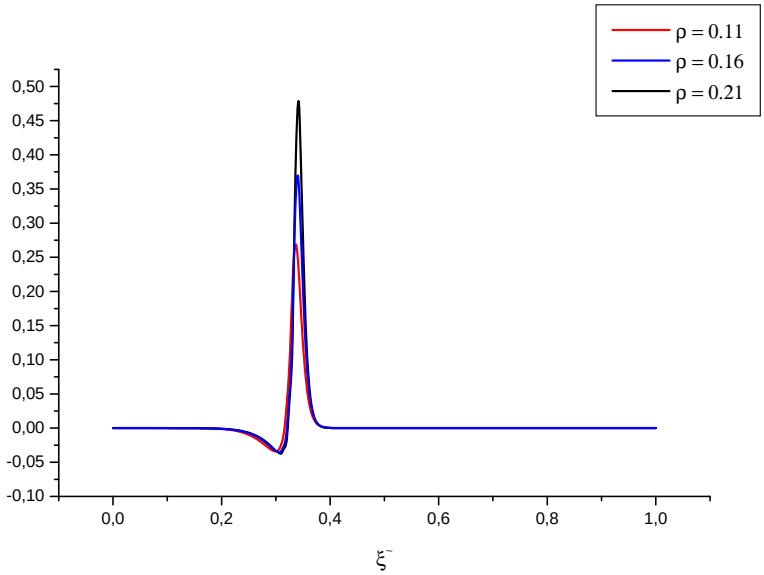

Fig. 16: The waveprofile v for multiple values of ρ with $\varepsilon = 0.08$.

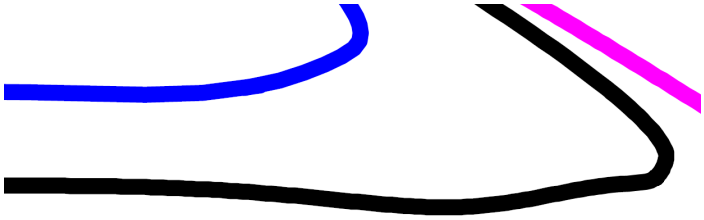

Fig. 17: Zoomed in after the turn in figure 14.

4.3 Difference between our results and Elmer and van Vleck's

Elmer and van Vleck have also done some research with the spatially discrete FitzHugh-Nagumo equations [14]. However, the nonlinear function used was a piecewise linear function f,

$$f(v) \equiv v - h(v-a), \text{ where } h(v-a) \equiv \begin{cases} 0, & v < a, \\ [0,1], & v = a, \\ 1, & v > a, \end{cases} \tag{4.24}$$

where $a \in (0,1)$. By using this function, Elmer and van Vleck could analytically find solutions to the equations, which in our case it is not possible to do so. The curves found by Elmer and van Vleck are monotonic decreasing in c travelling from top to bottom in contrast to the results in figure 14. In our case, both of our graphs grow in the $c-$direction after the turn.

5 Discussion and suggestions for further research

By looking at the Nagumo equation, we have found a relation between the α, ρ and the wavespeed c. For α small enough, there exists some values for ρ not equal to zero for which $c = 0$ holds. This is in contrast to the continuous case, where only $\rho = 0$ gives $c = 0$. As α becomes smaller, the interval for ρ in which $c = 0$ becomes larger. The profile of the wave for such ρ is not smooth.

Using the FitzHugh-Nagumo equations, which describe a pulse, we have plotted for some values of ε the relation between ρ and c. We found the solutions where c is close to c_*, with c_* the wavespeed belonging to the Nagumo equation. However, we also found solutions in which this is not the case and the theory discussed does not hold for those solutions. Krupa and Sandstede have describe how solutions of the PDE behave around the turning point in [13]. On the other hand, there is still not much known about the solutions after the turning point for the discrete case. Nevertheless, there is hope, since we can now find them numerically.

As mentioned before, it is not clear why we cannot find further solutions ($c > 0.44$) for the black graph at $c = 0.44$ in figure 14. Further research could give us the answer and also describe the behaviour of the solutions when c is not close to c_*.

References

[1] E. Decuypere, Hoofdstuk 5: Informatie-overdracht in fyshiologische processen. Deel A: zenuwcorrelatie. `http://www.biw.kuleuven.be/DP/fysiologie/hfdst5zpag1.htm`, 2005.

[2] L.C. Junqueira, J. Carneiro and R.O. Kelly, *Functionele histologie*. Elsevier gezondheidszorg, Maarssen, 2002.

[3] Keiichiro Susuki, *Myelin: A Specialized Membrane for Cell Communication*. Nature Education 3(9):59, 2010.

[4] Paul C. Fife and J.B. McLeod, *The Approach of Solutions of Nonlinear Diffusion Equations to Travelling Front Solutions*. Archive for Rational Mechanics and Analysis, Vol. 65, Issue 4, pp. 335-361, 1977.

[5] John Mallet-Paret, *The Global Structure of Traveling Waves in Spatially Discrete Dynamical Systems*. Journal of Dynamics and Differential Equations, Vol. 11, No. 1, 1999.

[6] H.J. Hupkes and S.M. Verduyn Lunel, *Analysis of Newton's Method to Compute Travelling Waves in Discrete Media*. Journal of Dynamics and Differential Equations, Vol. 17, Issue 3, pp. 523-572, 2005.

[7] Pankaj Kamthan, AUTO, SOFTWARE FOR CONTINUATION AND BIFURCATION PROBLEMS IN ORDINARY DIFFERENTIAL EQUATIONS. `http://indy.cs.concordia.ca/auto/`, 1996.

[8] Koen Engelborghs, DDE-BIFTOOL v. 2.03, a Matlab package for bifurcation analysis of delay differential equations. `http://twr.cs.kuleuven.be/research/software/delay/ddebiftool.shtml`, 2007.

[9] Christopher E. Elmer and Erik S. van Vleck, *A Variant of Newton's Method for the Computation of Traveling Waves of Bistable Differential-Difference Equations*. Journal of Dynamics and Differential Equations, Vol. 14, Issue 3, pp. 493-517, 2002.

[10] H. J. Hupkes and B. Sandstede, *Travelling Pulse Solutions for the Discrete FitzHugh-Nagumo System*. SIAM Journal on Applied Dynamical Systems, Vol.9, Issue 3, pp. 827-882, 2010.

[11] James P. Keener, *Propagation and Its Failure in Coupled Systems of Discrete Excitable Cells*. SIAM Journal on Applied Mathematics, Vol. 47, No. 3, pp. 556-572, 1987.

[12] Robert M. Miura, *Accurate Computation of the Stable Solitary Wave for the FitzHugh-Nagumo Equations*. Journal of Mathematical Biology, Vol. 13, Issue 3, pp. 247-269, 1982.

[13] Martin Krupa, Björn Sandstede and Peter Szmolyan, *Fast and Slow Waves in the FitzHugh-Nagumo Equation*. Journal of Differential Equations, Vol. 133, Issue 1, pp. 49-97, 1997.

[14] Christopher E. Elmer and Erik S. van Vleck, *Spatially discrete FitzHugh-Nagumo Equations*. Siam J. Appl. Math, Vol. 65, No. 4, pp. 1153-1174, 2005.